Crystal Structure and Luminescence Properties of Lead-Free Metal Halides: (C6H5CH2NH3)3MBr6 (M = Bi and Sb)

Journal:	*Journal of Materials Chemistry C*
Manuscript ID	TC-ART-02-2020-000562.R1
Article Type:	Paper
Date Submitted by the Author:	07-Mar-2020
Complete List of Authors:	Chen, Da; University of Science and Technology Beijing Dai, Fulong; University of Science and Technology Beijing Hao, Shiqiang; Northwestern University, Materials Science Zhou, Guojun; University of Science and Technology Beijing, School of Materials Science and Engineering Liu, Quanlin; University of Science and Technology Beijing, School of Materials science & engineering Wolverton, Chris; Northwestern University, Department of Materials Science and Engineering Zhao, Jing; University of Science and Technology Beijing, School of Materials Science and Engineering Xia, Zhiguo; South China University of Technology, School of materials science and engineering

Journal Name

ARTICLE

Crystal Structure and Luminescence Properties of Lead-Free Metal Halides: (C₆H₅CH₂NH₃)₃MBr₆ (M = Bi and Sb)

Crystal Structure and Luminescence Properties of Lead-Free Metal Halides: $(C_6H_5CH_2NH_3)_3MBr_6$ (M = Bi and Sb)

Da Chen[†], Fulong Dai[†], Shiqiang Hao[‡], Guojun Zhou[†], Quanlin Liu[†], Christopher Wolverton[‡], Jing Zhao[*,†], and Zhiguo Xia[*,†,⊥]

Organic–inorganic hybrid metal halides have received extensive attention owing to their versatile structures and optoelectronic properties. Herein, we report two lead-free metal halides, $(PMA)_3BiBr_6$ and $(PMA)_3SbBr_6$ [PMA⁺: $(C_6H_5CH_2NH_3)^+$, as the abbreviation of phenylmethylammonium], which possess iso-structural zero-dimensional structures and crystallize in the monoclinic space group $P2_1/c$. $(PMA)_3BiBr_6$ and $(PMA)_3SbBr_6$ exhibit optical band gaps of ~3.50 and 3.40 eV, respectively, and density functional theory calculations reveal their indirect bandgap behaviors. Upon 350 and 425 nm excitation, $(PMA)_3BiBr_6$ and $(PMA)_3SbBr_6$ exhibit broadband emission peaking at 510 nm and 625 nm with wide full-widths at half-maximum of ~153 and 175 nm, respectively. The emission mechanism of the metal halides is attributed to self-trapped exciton emission. The relationship between the crystal structure and luminescent efficiency is also discussed. Finally, both metal halides have high decomposition temperatures and are stable for long-term storage under ambient conditions, demonstrating their potential for optoelectronic applications.

1. Introduction

Recently, organic–inorganic metal halides (OIMHs) have attracted extensive attention, and great progress has been made in the field of material development, interface engineering, and device design. This can be attributed to the excellent optoelectronic properties of OIMHs originate from their band gap tunability, low defect density, long carrier lifetime, and high carrier mobility.[1] Moreover, their solution processability at room temperature makes OIMHs attractive for various applications,[2] including solar cells,[3] lasers,[4] photodetectors,[5] quantum dots,[6] and light-emitting diodes (LEDs).[7]

Despite the great potential of OIMHs for commercial application in solar cells and optoelectronic devices, two shortcomings should be addressed: (i) most OIMHs contain highly toxic Pb element and (ii) the instability against moisture and temperature shortens the lifetime of the devices. Two approaches have been proposed to overcome these issues: (i) the design of

lead-free metal halides by replacing Pb^{2+} with other cations and (ii) the exploration of low-dimensional metal halide materials by introducing hydrophobic macromolecular organic cations. Specifically, for approach (i), attempts have been made to replace Pb^{2+} with less toxic Sn^{2+} or Ge^{2+}; however, both Sn^{2+} and Ge^{2+} are easily oxidized to Sn^{4+} and Ge^{4+} in air.[8, 9] In addition, monovalent and trivalent cations can be used to replace Pb^{2+} to synthesize double perovskite with the general formula of $A_2B'B''X_6$ (A = $CH_3NH_3^+$, Cs^+; B' = Ag^+, Cu^+; B'' = Bi^{3+}, Sb^{3+}, In^{3+}).[10] Bi^{3+} or Sb^{3+} and a vacancy co-substitution of Pb^{2+} is another appealing option, as Bi^{3+} and Sb^{3+} possess the same electronic structure as Pb^{2+},[11, 12] preserving the advantages of Pb^{2+} with highly anisotropic electronic behavior, low conduction-band effective mass, and high electron mobility.[13, 14] For approach (ii), the blocky organic cations can cut the inorganic octahedra into 2-, 1-, or even 0-dimensional structures.[15] This reduction of the dimension is beneficial for improving the stability.[16] Additionally, low-dimensional structures can induce efficient wide-band luminescence, which originates from the enhanced self-trapped excitons (STEs).[17, 18] These approaches provide various options for improving metal halides in terms of the structural dimension and the selection of organic cations.

Under the guidance of the above ideas, we selected Bi^{3+}/Sb^{3+} and $C_6H_5CH_2NH_3^+$ [phenylmethylammonium abbreviated as PMA⁺] to design new low-dimensional OIMHs and study the photoelectric properties. Presently, some Sb- or Bi- based OIMHs

[†] The Beijing Municipal Key Laboratory of New Energy Materials and Technologies, School of Materials Sciences and Engineering, University of Science and Technology Beijing, Beijing 100083, China.
[‡] Department of Materials Science and Engineering, Northwestern University, Evanston, Illinois 60208, United States.
[⊥] State Key Laboratory of Luminescent Materials and Devices and Institute of Optical Communication Materials, South China University of Technology, Guangzhou 510641, China

have been reported to show great potential for optoelectronic applications, such as $(C_4N_2H_{14}Br)_4SnX_6$ (X = Br, I)[16] and $(C_8NH_{12})_4Bi_{0.57}Sb_{0.43}Br_7·H_2O$.[19] Other reported Sb- and Bi-based OIMHs include $(CH_3NH_3)_3Sb_2I_9$,[20] $(C_6H_{20}N_3)BiI_6·H_2O$,[21] $(C_5H_{10}N)_2BiBr_5$,[22] $(C_7H_7)MI_4$ (M = Bi or Sb),[23] $(C_7H_{10}NO)_2BiBr_5$,[24] $(C_7H_{18}N_2O)_3Sb_4I_{18}·H_2O$,[25] and $(C_7H_{18}N_2O)Sb_2I_8·H_2O$;[25] however, despite their crystal structures being reported, their luminescent properties have not yet been comprehensively studied.

Herein, we prepared two environmentally friendly lead-free 0-dimensional (0D) OIMHs with the chemical formula $(PMA)_3BiBr_6$ (**1**) and $(PMA)_3SbBr_6$ (**2**) using a facile solution method. Both compounds exhibit typical semiconducting behavior with experimental band gaps of ~3.50 and 3.40 eV for **1** and **2**, respectively. Upon 350 and 425 nm excitation, large Stokes-shifted broadband emission was detected, with very wide full-widths at half-maximum (FWHMs). In addition, both compounds exhibited good thermal and ambient stability. The luminescent mechanism of **1** and **2** and the relationship between the crystal structure and luminescent efficiency are discussed in detail.

2. Experimental section

Synthesis. Materials. Phenylmethylammonium bromide (PMABr) (≥99.5%) was purchased from Xi'an Polymer Light Technology Corp. Bismuth(Ⅲ) bromide (BiBr$_3$) (99.9%) and antimony(Ⅲ) bromide (SbBr$_3$) (99.9%) were purchased from Aladdin Company. Hydrogen bromide (HBr) (48 wt.% in H$_2$O) was purchased from Beijing Chemical Works.

Synthesis of **1**. The stoichiometric mixture of PMABr (0.334 g) and BiBr$_3$ (0.266 g) was dissolved in 4.6 mL of HBr under heating and continuous stirring at ~92 °C. After all the reactants dissolved in the solution, an orange-yellow solution was obtained, which was slowly cooled to ~25 °C. Finally, light-yellow, long rod-like crystals with sizes up to 1 cm were obtained. The yield of the reaction based on Bi element was ~72%.

Synthesis of **2**. The stoichiometric mixture of PMABr (0.366 g) and SbBr$_3$ (0.234 g) was dissolved in 4.8 mL of HBr and heated to 92 °C under continuous stirring, forming a light-yellow solution, which was slowly cooled to ~25 °C. Finally, large bulk light-yellow crystals with sizes up to 1 cm were obtained. The yield of the reaction based on Sb element was ~60%.

Characterization. A selected single crystal was subjected to X-ray diffraction (XRD) analysis using a Rigaku XtaLAB PRO single-crystal diffractometer with Mo Kα radiation. XPREP software was used to determine the crystal structure using the direct method, and the SHELXTL package was used for structure refinement.[26] Powder X-ray diffraction (PXRD) patterns were collected using a D8 Advance powder diffractometer (Bruker Corporation, Germany) equipped with a Cu Kα irradiation source, operating at 40 kV and 40 mA. Scanning electron microscopy (SEM) and energy-dispersive X-ray spectroscopy (EDS) analysis were performed using a JEOL JSM-

6510A scanning electron microscope. Thermogravimetric analysis (TGA) was performed using a Setaram Labsys Evo at a heating rate of 10 °C/min with a maximum temperature of 500 °C. Absorption spectra were collected using an ultraviolet–visible–near-infrared (UV–vis–NIR) spectrophotometer (Hitachi UH4150) at room temperature. Steady-state photoluminescence (PL) spectra and luminescence decay curves were obtained using a FLSP9200 fluorescence spectrophotometer (Edinburgh Instruments Ltd., U.K.) with a PMT detector and a 150-W Xe lamp.

DFT calculation. Density functional theory (DFT) calculation was performed using periodic boundary conditions and a plane-wave basis set as implemented in the Vienna *ab initio* simulation package.[27] The DFT calculations were converged to approximately 3 meV/cation using a basis set energy cutoff of 500 eV and dense k-meshes corresponding to 4000 k-points per reciprocal atom in the Brillouin zone.

3. Results and Discussion

Synthetic Methods. Both compounds exhibited good crystal quality, with crystal sizes reaching the centimeter level (Figure 1). They were synthesized via direct combination of the organic cation precursor and MBr$_3$ (M = Bi or Sb) in an aqueous solution of HBr at 92 °C followed by slow cooling of the solution to ~25 °C at a cooling rate of 1.0 °C/h. Figure S1 presents SEM images and EDS analysis results of compounds **1** and **2**. The EDS elemental analysis indicates that the atomic ratio of M:Br (M = Bi, Sb) is approximately 1:5.6, which is consistent with the crystallographic analysis.
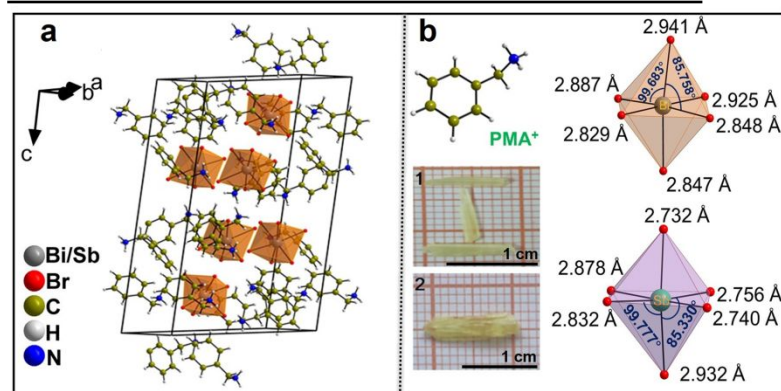

Figure 1. (a) Crystal structure of **1** and **2**. (b) Structure of organic cation of PMA$^+$, photographs of single crystals of **1** and **2**, and distorted octahedra in **1** and **2**, respectively.

Crystal Structure. Compounds **1** and **2** are isostructural, and the unit cells and detailed crystallographic data are shown in Table 1. Both compounds crystallized in the monoclinic space group $P2_1/c$; other structural details (Table S1–S8) and crystallographic information files (CIFs) for **1** and **2** are presented in the Supporting Information. As illustrated in Figure 1a, compounds **1** and **2** possess a 0D structure with isolated octahedra. Each Bi is

coordinated with six adjacent Br atoms, forming distorted octahedra with bond lengths ranging from 2.829 to 2.941 Å (Figure 1b). These bond lengths are in the same range as those reported for $[C_6H_{20}N_3]BiBr_6 \cdot H_2O$ (2.829–2.8643 Å) and $C_4H_{16}N_3BiBr_6$ (2.829–2.8643 Å).[28, 29] The Br–Bi–Br bond angles range from 85.75° to 99.69° (Figure 1b). The deviation of these values from 90° indicates that the inorganic octahedra are distorted. In compound **2**, the Sb–Br bond length ranges from 2.732 to 2.932 Å (Figure 1b), which is slightly shorter than the Bi–Br bond length; this result is consistent with the Shannon radii of 1.03 Å for Bi and 0.76 Å for Sb in six coordination environments.[30] The Br–Sb–Br angle ranges from 85.33° to 99.77°, which also indicates that the inorganic octahedra are distorted (Figure 1b).

Comparing **1** and **2** with the reported $(C_6H_5CH_2CH_2NH_3)_3BiBr_6$ with $I2/a$ space group, all of them belong to the centrosymmetric monoclinic system with 0D structure consisting of alternating $[MBr_6]^{3-}$ (M = Bi or Sb) octahedra and organic cations linked by hydrogen bonding. As illustrated in Figure S2, the hydrogen bond length ranges from 2.541 to 2.986 Å (Figure S2a) for compound **1** and from 2.556 to 2.990 Å (Figure S2b) for compound **2**, which are in accordance with the bond lengths reported for $[(CH_3)_2NH_2]_6(BiBr_6)_2$ (2.500–2.770 Å),[31] $(C_6H_{20}N_3)BiBr_6 \cdot H_2O$ (2.440–3.110 Å),[28] and $(C_7H_{10}NO)_2BiBr_5$ (2.470–2.980 Å).[24]

Table 1. Crystal data and structure refinement of **1** and **2** at 100(2) K.

Compound	(PMA)$_3$BiBr$_6$	(PMA)$_3$SbBr$_6$
Empirical formula	$(C_6H_5CH_2NH_3)_3BiBr_6$	$(C_6H_5CH_2NH_3)_3SbBr_6$
Formula weight	1011.91	925.69
Temperature	100(2) K	100(2) K
Wavelength	0.71069 Å	0.71073 Å
Crystal system	monoclinic	monoclinic
Space group	$P2_1/c$	$P2_1/c$
Unit cell dimensions	a = 15.425 Å, α = 90°	a = 15.2246 Å, α = 90°
	b = 8.174 Å, β = 99.56°	b = 8.0632 Å, β = 100.005°
	c = 24.610 Å, γ = 90°	c = 24.3042 Å, γ = 90°
Volume	3059.6 Å^3	2938.19 Å^3
Z	4	4
Density (calculated)	2.197 g/cm^3	2.093 g/cm^3
Absorption coefficient	13.612 mm^{-1}	9.113 mm^{-1}
F(000)	1876	1752
ϑ range for data collection	2.314 to 25.00°	1.984° to 29.346°
Index ranges	-18<=h<=18, -9<=k<=9,	-18<=h<=20, -10<=k<=10,
	-29<=l<=29	-32<=l<=32
Reflections collected	25982	35727
Independent reflections	5375 [R_{int} = 0.0553]	7269 [R_{int} = 0.0304]

Completeness to ϑ =25.00°	99.7%	100%
Refinement method	Full-matrix least-squares on F^2	
Data / restraints / parameters	5378 / 10 / 283	7296 / 18 / 283
Goodness-of-fit	1.130	1.019
Final R indices [$I > 2\sigma$(I)]	R_{obs} = 0.0801, wR_{obs} = 0.1869	R_{obs} = 0.0334, wR_{obs} = 0.0559
R indices [all data]	R_{all} = 0.1019, wR_{all} = 0.2023	R_{all} = 0.0506, wR_{all} = 0.0593
Largest diff. peak and hole	2.770 and -0.836 e·Å^{-3}	0.673 and -0.648 e·Å^{-3}

$R = \Sigma||F_o|-|F_c|| / \Sigma|F_o|$, $wR = \{\Sigma[w(|F_o|^2 - |F_c|^2)^2] / \Sigma[w(|F_o|^4)]\}^{1/2}$ and $w = 1/[\sigma^2(F_o^2)+(0.0462P)^2]$ where $P=(F_o^2+2F_c^2)/3$

Stability Studies. The experimental PXRD patterns of **1** and **2** and calculated patterns based on single-crystal structures are compared in Figure 2a–b. The experimental PXRD and calculated peaks fit well, and no extra peaks were observed, indicating the high purity of the obtained samples. In addition, we compared the PXRD patterns of **1** and **2** samples stored in air for 3 months to those of the as-synthesized samples. No peak position or intensity changes were observed, indicating that both **1** and **2** are stable in air.
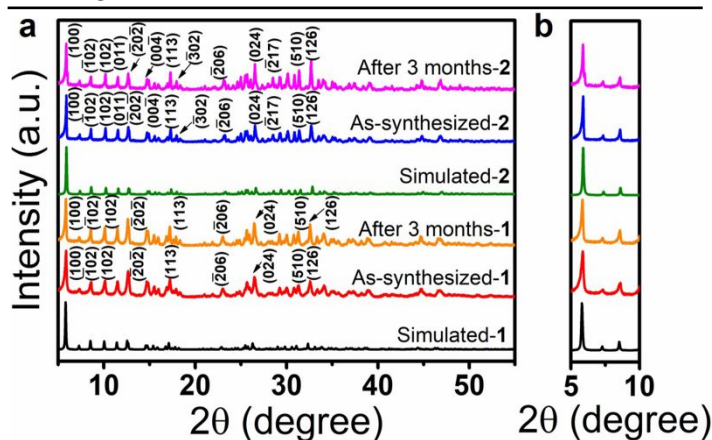

Figure 2. (a) Comparison of calculated PXRD patterns based on SXRD data and experimental PXRD patterns of polycrystalline powders of **1** and **2** measured on fresh samples and after storing in air for 3 months. (b) Selected diffraction peaks in the range of 5°–10° of **1** and **2**.

To investigate the thermal stability of the two compounds at elevated temperature, TGA measurements were conducted under nitrogen flow from room temperature to 500 °C. Sample **1** was stable below ~273 °C, and a multiple-step decomposition profile was obtained for the compound (Figure 3a). In the first stage, approximately 32% of the initial weight was lost, which can be attributed to volatilization of the PMA ($C_6H_5CH_2NH_2$) (the theoretical calculation is approximately 32.00%). There is an obvious platform when the temperature is higher than 325 °C, and until 325 °C, the weight loss was approximately 61%. To verify the residual content, fresh samples were heated to 325 °C in

a muffle furnace and held for 2 h; then, the residues were collected and examined using PXRD (Figure S3). After searching in the Cambridge Crystallographic Data Centre (CCDC) database, the product was identified as a mixture of $BiBr_3$ and Bi_6Br_7. Thus, the weight loss of sample **1** may be attributed to the volatilization of PMA and subsequently Br_2. TGA revealed that compound **2** was stable up to ~232 °C (Figure 3b), showing a two-step decomposition. After the first step, it lost about ~35% of the initial weight, corresponding to the volatilization of PMA with a calculated value of ~35.02%. After the second step, only 18% of the weight remained.

Compounds **1** and **2** exhibited higher thermal stability than reported OIMHs with small organic molecules such as $MA_3Bi_2Br_9$, $(C_5H_{10}N)_2BiBr_5$, and $(C_8NH_{12})_4Bi_{0.57}Sb_{0.43}Br_7 \cdot H_2O$, which start to decompose at approximately 200 °C, 140 °C, and 120 °C, respectively.[19, 22, 32] Thus, the thermal stability of OIMHs containing large organic molecules appears to be higher than those containing small organic molecules.
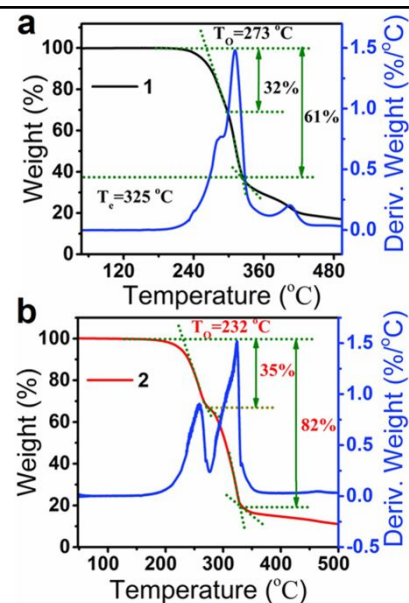

Figure 3. TGA data for powder samples of **1** (a) and **2** (b) under N_2 atmosphere.

Optical Properties and DFT Calculations. The Raman spectra of compound **1** was studied by Fehlner et al.[33], but no structure or other properties were characterized. Herein, the spectroscopic properties of both **1** and **2** were investigated in detail. Figure 5a presents the absorption spectra of polycrystal powders **1** and **2** and the band gaps of **1** and **2** were estimated to be ~3.50 and ~3.40 eV, respectively. As illustrated in Figure 5a, the absorption peaks are slightly lower than the band gaps of compounds **1** and **2** corresponding to the exciton absorption peaks with peak energies of ~3.28 and 3.38 eV, respectively, at room temperature. The presence of sharp exciton peaks at room temperature indicates that the compound has high exciton binding energy.[34] The absorption band at higher energy corresponds to the interband absorption. These absorption peaks are similar to those of previously reported OIMH compounds, including $[(CH_3)_2NH_2]_3[BiI_6]$ (~2.60 and 3.04 eV),[35] $(C_6H_{20}N_3)BiBr_6 \cdot H_2O$ (~2.36 and 3.10 eV),[28] $C_4H_{16}N_3BiBr_6$ (~3.22 and 4.08 eV),[29] and $[(CH_3)_2NH_2]_6(BiBr_6)_2$ (~3.30 and 3.97 eV)[31].

The specific bandgap types were determined by DFT calculation. The band structures of compounds **1** and **2** consist of indirect (*H* to *X*) bandgaps of 3.24 and 2.77 eV, respectively, thus exhibiting weak PL emission (Figure 4a, b). For compound **1**, the valence band maximum (VBM) consists of Bi 6s and Br 4p states at *H*, and the conduction band minimum (CBM) consists of Bi 6p and Br 4p states at *X* (Figure 4c). Similarly, the VBM of **2** mainly consists of Sb 5s and Br 4p states at *H*, and the CBM consists of Sb 5p and Br 4p states at *X* (Figure 4d).
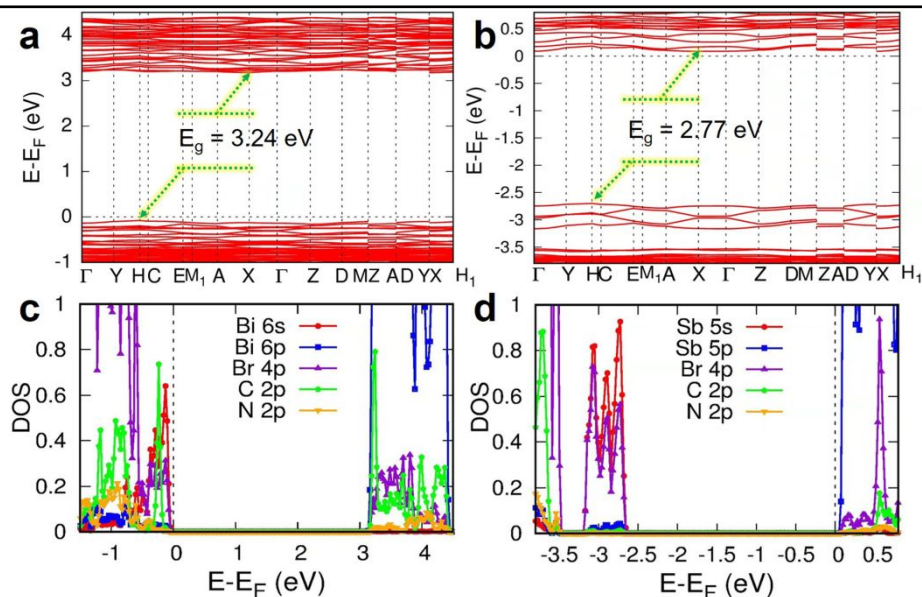

Figure 4. Band structures of **1** (a) and **2** (b). Density of states of **1** (c) and **2** (d).

Figure 5b presents the normalized PL emission spectra of compounds **1** and **2**. Upon 350 nm excitation, the PL spectrum of compound **1** exhibited two broad emission band peaking at 405 and 510 nm; and the one with low energy is much stronger and processes a large Stokes shift of 160 nm and a FWHM of ~153 nm. Upon the excitation of 425 nm light, the PL spectrum of compound **2** also exhibited two bands peaking at 453 and 625 nm, and the one with low energy is stronger with a large Stokes shift of 200 nm and a large FWHM of ~175 nm. This broad emission is commonly observed in low-dimensional OIMHs with strong electron–phonon coupling.[19, 36] For example, $(C_8NH_{12})_4Bi_{0.57}Sb_{0.43}Br_7 \cdot H_2O$ exhibits white light emission with a FWHM of ~160 nm,[19] and $(C_6H_{20}N_3)BiBr_6 \cdot H_2O$ exhibits broadband emission with a FWHM of ~154 nm.[28]

In order to explore the emission mechanism, experiments were conducted on the dependence of emission intensity and excitation power. As shown in Figure 5c, a linear relationship without saturation is observed, which indicates that the broadband emission does not originate from permanent defects.[37] In addition, the PL spectrum of the staring material PMABr was collected under the same conditions to prove that the luminescence does not come from the emission of organic molecules. The emission band of PMABr peaks at 425 nm (Figure S4) that is very different from the emission characteristics of compounds **1** and **2**. The PL spectra of the two compounds can be attributed to singlet and triplet emissions of isolated ns^2 metal centers, which are also known as self-trapping excitons (STE) emission. In present work, the ground state is $^1S_0$ (here are $6s^2$ or $5s^2$ of Bi^{3+} or Sb^{3+}), and the excited states are derived from the $6s6p$ (Bi^{3+}) or $5s5p$ (Sb^{3+}) orbit, which split into four levels, namely $^1P_1$, $^3P_0$, $^3P_1$, and $^3P_2$.[38] According to the transition rules, the high energy emission bands of **1** and **2** peaking at 405 and 453 nm, respectively, are attributed to the $^1P_1 \rightarrow {}^1S_0$ transition (Figure 5d). The low energy broadband emission of compounds **1** and **2** peaking at 510 and 625 nm, respectively, are attributed to the $^3P_n \rightarrow {}^1S_0$ (n = 0, 1, 2) transitions owing to intersystem crossing (ISC). This ISC is accelerated in heavy elements due to larger spin-orbit coupling (SOC), leading to the mixing of ^1P and ^3P states. These emissions are previously discussed in the compounds of

Bmpip$_2$MBr$_4$ (Bmpip is the abbreviation of 1-butyl-1-methyl-piperidinium, M = Ge, Sn, Pb)[39] and Cs$_2$SnCl$_6$:Sb^{3+} (Sb/Sn = 0.1).[40] Upon higher energy photoexcitation at 330 and 400 nm for compound **1** and **2**, respectively, the high energy emission from singlet state become stronger (Figure S5), which is in accordance with that reported by Morad, V. et al.[39] The luminescence decay curves of **1** and **2** are shown in Figure S6. Due to the low PL intensity, only the lifetimes of the triplet broadband emissions are detected, which are 1.031 and 1.508 ns for **1** and **2**, respectively. The triplet lifetime is short, which is the result of a mixture of singlet and triplet states. This can be verified with a relatively small Stokes shift of 1.11 eV of **1** and 0.94 eV of **2**.[39] The CIE color coordinates of **1** and **2** are (0.3118, 0.4164) and (0.4981, 0.4445), respectively (Figure 5e).

Figure S7 present the PL spectra of **1** and **2** at low temperatures, respectively. As the temperature decreases, the intensity of the emissions increase monotonically, which can be attributed to the reduction of the nonradiative decay. With increasing temperature, the

band widening of compounds **1** and **2** can be observed, and the increase of the FWHM can be described by the following law:[41]

$$f(T) = 2.36 \times \sqrt{S} \times E_{ph} \times \left[\coth\left(\frac{E_{ph}}{2kT}\right) \right]^{1/2} ,$$

where $f(T)$ is the FWHM at different temperatures, S is the Huang–Rhys parameter, k is the Boltzmann constant, and E_{ph} is the effective phonon energy. The fitting results are presented in Figure S7c-d, and the FWHM shows thermal dependence. We can determine that compound **1** has S = 13.7 and E_{ph} = 83.2 meV and that compound **2** has S = 12.5 and E_{ph} = 56.9 meV. The S values of compounds **1** and **2** are larger than those of inorganic compounds, such as 6.4 for SrSe,[42] 8.4 for Y$_3$Al$_5$O$_{12}$,[43] and 9.0 for Lu$_3$Al$_5$O$_{12}$,[44] indicating that **1** and **2** have strong electron–phonon coupling. Moreover, the values of E_{ph} are much higher than those of all-inorganic metal halides, such as Cs$_3$Bi$_2$I$_6$Cl$_3$ (E_{ph} = 4.0 meV)[45] and Cs$_2$AgInCl$_6$ (E_{ph} = 17.4 meV),[46] implying that the energies of the lattice vibration for **1** and **2** are relatively large and the structural rigidity is relatively weak.
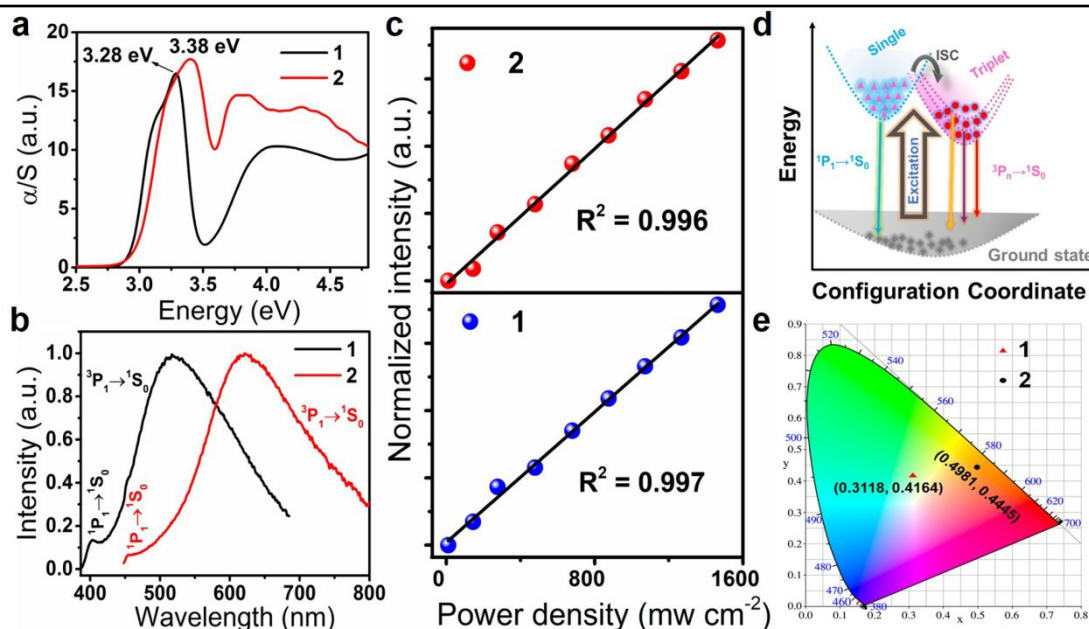

Figure 5. (a) Optical absorption spectra. (b) PL spectra upon 350 and 425 nm excitation of **1** and **2** at room temperature, respectively. (c) Emission intensity versus excitation power for **1** and **2** at room temperature. (d) Mechanism diagram of photoluminescence for **1** and **2**. (e) CIE color coordinates of **1** and **2** in 1931 color space chromaticity diagram.

Both compounds **1** and **2** exhibit relatively weak PL intensity compared with that of their In-based analogue (PMA)$_3$InBr$_6$, which exhibited a PLQY of ~35%.[47] To reveal the structural effects of PL intensities in these 0D compounds, we compared our result with those for other previously reported 0D compounds with six coordinated s^2 metal cations. First and foremost, the effect of the band nature should be considered. (PMA)$_3$InBr$_6$ is isostructural with **1** and **2**, showing an efficient broadband orange emission with the mechanism of STE emission. DFT calculation indicated that (PMA)$_3$InBr$_6$ possesses a direct bandgap. Thus, comparing with indirect-band-gap compounds **1** and **2**, in light of the absorption process of (PMA)$_3$InBr$_6$, no phonon processes

are needed, which is more efficient, resulting in higher PLQY. In addition, previous works have shown that the formation of the STE states of OIMHs with the same structure dimensionality may be related to the distortion level of the metal coordination geometry, and also related to many other factors, such as the structural disorder, organic molecules, PL quenching temperature, etc.[48, 49] Herein, it is of interest to discuss the PL characterization and structural relationship of (PMA)$_3$MBr$_6$ (M = Bi, Sb, In). With the purpose of characterizing the difference in octahedral distortion, we defined the distortion based on the M–X bond length and X–M–X (M and X are metal cations and halogen anions) angle variance:[50]

$$\lambda_{oct} = \frac{1}{6}\sum_{n=1}^{6}[(d_n - d_0)/d_0]^2$$

$$\sigma^2 = \frac{1}{11}\sum_{n=1}^{12}(\theta_n - 90°)^2$$

where d_n are six individual M–X bond lengths, d_0 is the average of the M–X bond distance, and θ_n are the bond angles of each X–M–X. The results are tabulated in Table 2.

Table 2. Summary of Bandgap behavior, PL emission, FWHM, bond length distortions, angle variance and PLQY for title compounds and 0D compounds with six coordinated metal cations reported in the literature.

Compound	Bandgap behavior	PL (nm)	FWHM (nm)	λ_{oct} (*10^{-4})	σ^2	PLQY	Ref.
$(PMA)_3BiBr_6$	indirect	510	153	2.1	14.57	<1%	This work
$(PMA)_3SbBr_6$	indirect	640	175	7.1	14.60	<1%	This work
$(C_4N_2H_{14}Br)_4SnBr_6$	direct	570	105	45.69	18.20	95%	16
$(Ph_4P)_2SbCl_5$	direct	648	136	64.5	8.20	87%	51
$(C_4N_2H_{14}Br)_4SnI_6$	direct	620	118	1.57	19.45	75%	16
$(PMA)_3InBr_6$	direct	610	132	1.1	4.99	35%	47
$(C_3N_3H_{11}O)_2PbBr_6·4H_2O$	direct	568	200	0.00438	2.57	9.3%	52
$(C_8NH_{12})_4Bi_{0.57}Sb_{0.43}Br_7·H_2O$	direct	450, 640	400 ~ 850	5.94	8.04	4.5%	19
$(C_8NH_{12})_4BiBr_7·H_2O$	-	450	-	12.34	10.62	0.7%	19

In Table 2, we can find that with a direct band gap and very large structural distortion, $(C_4N_2H_{14}Br)_4SnBr_6$[16], $(Ph_4P)_2SbCl_5$[51] (Ph_4P is tetraphenylphosphonium cation) and $(C_4N_2H_{14}Br)_4SnI_6$[16] exhibit very high PL emission efficiency. However, PLQY is not linearly related to the degree of structural distortion. For example, $(PMA)_3InBr_6$ with less distorted structure than $(C_8NH_{12})_4Bi_{0.57}Sb_{0.43}Br_7·H_2O$[19] but higher PLQY; and $(C_3N_3H_{11}O)_2PbBr_6·4H_2O$[52] possesses a distortion level lower than $(C_8NH_{12})_4Bi_{0.57}Sb_{0.43}Br_7·H_2O$ but higher PLQY.

To compare the PL intensities of compounds **1** and **2** (Figure S8), PL spectra were obtained under exactly the same conditions. The PL intensity of **2** is much larger than that of **1** (Figure S8), which correlates well with the distortion level of compound **2** ($\lambda_{oct} = 7.1 \times 10^{-4}$ and $\sigma^2 = 14.60$) being greater than that of compound **1** ($\lambda_{oct} = 2.1 \times 10^{-4}$ and $\sigma^2 = 14.57$). Notably, the distortion degrees of **1** and **2** are larger than that of $(PMA)_3InBr_6$, which may theoretically indicate stronger emission than the latter, provided that the band gaps of **1** and **2** can be tuned to be direct ones through doping.

4. Conclusions

In summary, we prepared two new lead-free OIMHs $(PMA)_3BiBr_6$ (**1**) and $(PMA)_3SbBr_6$ (**2**), which crystallized in the monoclinic space group $P2_1/c$. The two compounds are isostructural 0D structures and are composed of discrete octahedra and organic cations linked by hydrogen bonding. The DFT calculations revealed the indirect band gap behavior of **1** and **2**, and the optical band gap was experimentally determined to be ~3.50 and 3.40 eV, respectively. Both compounds **1** and **2** exhibited good ambient stability and relatively high decomposition temperatures under N_2 gas flow (> 230 °C). Upon 350 and 425 nm excitation, compound **1** and **2** exhibited large Stokes-

shifted dual broad PL emission with the FWHMs of ~153 and 175 nm, respectively. This broad emission in the 0D Bi- and Sb-based OIMHs is attributed to STE (singlet and triplet) emission. The thermal dependence of the FWHM was discussed in detail. The discovery of environmentally stable **1** and **2** and their photoluminescence properties further demonstrate the importance of lead-free low-dimensional OIMHs for optoelectronic applications.

Supporting Information

The Supporting Information is available free of charge on the RSC Publications website at http://www.rsc.org/.

Crystal structure of **1** and **2**; Tables of atomic coordinates, displacement parameters, anisotropic displacement parameters, and bond distances of **1** and **2** (Table S1–S8); SEM and EDS results, N–H···Br hydrogen bonding of **1** and **2**, XRD analysis of **1** after the first step decomposition, PLE and PL spectra of PMABr at room temperature, PL spectra excited by higher energy photoexcitation for compounds **1** and **2**, PL decay curves of compound **1** and **2** polycrystalline powder at room temperature, temperature-dependent steady-state PL spectra of **1** and **2**, fitting of the FWHM for compound **1** and **2** as a function of temperature, temperature-dependent normalized steady-state PL spectra of **1** and **2**, PL spectra of **1** and **2** at 350 K and 80 K. comparison of PL spectra of **1** and **2** (Figure S1–S8).

Corresponding Author

* jingzhao@ustb.edu.cn

* xiazg@ustb.edu.cn

Conflicts of interest

There are no conflicts to declare.

Acknowledgements

Notes and references

1. D. Shi, V. Adinolfi, R. Comin, M. Yuan, E. Alarousu, A. Buin, Y. Chen, S. Hoogland, A. Rothenberger, K. Katsiev, Y. Losovyj, X. Zhang, P. A. Dowben, O. F. Mohammed, E. H. Sargent and O. M. Bakr, *Science*, 2015, **347**, 519.

2. Z. Song, J. Zhao and Q. Liu, *Inorg. Chem. Fron.*, 2019, **6**, 2969-3011.

3. M. Kim, G.-H. Kim, T. K. Lee, I. W. Choi, H. W. Choi, Y. Jo, Y. J. Yoon, J. W. Kim, J. Lee, D. Huh, H. Lee, S. K. Kwak, J. Y. Kim and D. S. Kim, *Joule*, 2019, **3**, 2179-2192.

4. Q. Zhang, S. T. Ha, X. Liu, T. C. Sum and Q. Xiong, *Nano. Lett.*, 2014, **14**, 5995-6001.

5. L. Dou, Y. M. Yang, J. You, Z. Hong, W. H. Chang, G. Li and Y. Yang, *Nat. Commun.*, 2014, **5**, 5404.

6. M. Leng, Z. Chen, Y. Yang, Z. Li, K. Zeng, K. Li, G. Niu, Y. He, Q. Zhou and J. Tang, *Angew. Chem., Int. Ed.*, 2016, **55**, 15012-15016.

7. N. Wang, L. Cheng, R. Ge, S. Zhang, Y. Miao, W. Zou, C. Yi, Y. Sun, Y. Cao, R. Yang, Y. Wei, Q. Guo, Y. Ke, M. Yu, Y. Jin, Y. Liu, Q. Ding, D. Di, L. Yang, G. Xing, H. Tian, C. Jin, F. Gao, R. H. Friend, J. Wang and W. Huang, *Nat. Photonics.*, 2016, **10**, 699-704.

8. F. Hao, C. C. Stoumpos, D. H. Cao, R. P. H. Chang and M. G. Kanatzidis, *Nat. Photonics.*, 2014, **8**, 489-494.

9. C. C. Stoumpos, L. Frazer, D. J. Clark, Y. S. Kim, S. H. Rhim, A. J. Freeman, J. B. Ketterson, J. I. Jang and M. G. Kanatzidis, *J. Am. Chem. Soc.*, 2015, **137**, 6804-6819.

10. X. Zhao, L. Zhang, Z. Xiao and Y. Sun, *Joule*, 2018, **2**.

11. P. C. Harikesh, H. K. Mulmudi, B. Ghosh, T. W. Goh, Y. T. Teng, K. Thirumal, M. Lockrey, K. Weber, T. M. Koh, S. Li, S. Mhaisalkar and N. Mathews, *Chem. Mater.*, 2016, **28**, 7496-7504.

12. J.-C. Hebig, I. Kühn, J. Flohre and T. Kirchartz, *ACS Energy. Letter.*, 2016, **1**, 309-314.

13. G. G. Briand, N. Burford, M. D. Eelman, N. Aumeerally, L. Chen, T. S. Cameron and K. N. Robertson, *Inorg. Chem.*, 2004, **43**, 6495-6500.

14. X.-y. Liu, J.-h. Zeng, S.-y. Zhang, R.-b. Zheng, X.-m. Liu and Y.-t. Qian, *Chem. Phys. Lett.*, 2003, **374**, 348-352.

15. D. H. Cao, C. C. Stoumpos, O. K. Farha, J. T. Hupp and M. G. Kanatzidis, *J. Am. Chem. Soc.*, 2015, **137**, 7843-7850.

16. C. Zhou, H. Lin, Y. Tian, Z. Yuan, R. Clark, B. Chen, L. J. van de Burgt, J. C. Wang, Y. Zhou, K. Hanson, Q. J. Meisner, J. Neu, T. Besara, T. Siegrist, E. Lambers, P. Djurovich and B. Ma, *Chem. Sci.*, 2018, **9**, 586-593.

17. S. Tomimoto, H. Nansei, S. Saito, T. Suemoto, J. Takeda and S. Kurita, *Phys. Rev. Lett.*, 1998, **81**, 417-420.

18. Y. Wada, U. Lemmer, E. O. Göbel, M. Yamashita and K. Toriumi, *Phys. Rev. B.*, 1995, **52**, 8276-8282.

19. R. Zhang, X. Mao, Y. Yang, S. Yang, W. Zhao, T. Wumaier, D. Wei, W. Deng and K. Han, *Angew. Chem., Int. Ed.*, 2019, **58**, 2725-2729.

20. N. Elfaleh and S. Kamoun, *J. Organomet. Chem.*, 2016, **819**, 95-102.

21. J. Zaleski, R. Jakubas, L. Sobczyk and J. Mróz, *Ferroelectrics*, 1990, **103**, 83-90.

22. W. Masmoudi, S. Kamoun, H. F. Ayedi and K. Guidara, *Physica. B.*, 2012, **407**, 2365-2371.

23. I. W. H. Oswald, E. M. Mozur, I. P. Moseley, H. Ahn and J. R. Neilson, *Inorg. Chem.*, 2019, **58**, 5818-5826.

24. Z. Aloui, V. Ferretti, S. Abid, F. Lefebvre, M. Rzaigui and C. Ben Nasr, *J. Mol. Struct.*, 2016, **1118**, 301-306.

25. Y. Li, Z. Xu, X. Liu, K. Tao, S. Han, Y. Wang, Y. Liu, M. Li, J. Luo and Z. Sun, *Inorg. Chem.*, 2019, **58**, 6544-6549.

26. G. M. Sheldrick, *Acta Crystallogr., Sect. A: Found. Crystallogr.*, 2008, **64**, 112-122.

27. G. Kresse and J. Furthmüller, *Phys. Rev. B*, 1996, **54**, 11169-11186.

28. N. Elfaleh and S. Kamoun, *J. Mol. Struct.*, 2014, **1075**, 479-485.

29. H. Dammak, H. Feki, H. Boughzala and Y. Abid, *Spectrochim. Acta. A. Mol. Biomol. Spectrosc.*, 2015, **137**, 1235-1243.

30. R. Shannon, *Acta. Crystallogr. A.*, 1976, **32**, 751-767.

31. A. Ben Ahmed, H. Feki and Y. Abid, *Spectrochim. Acta. A. Mol. Biomol. Spectrosc.*, 2014, **133**, 357-364.

32. M. Leng, Y. Yang, K. Zeng, Z. Chen, Z. Tan, S. Li, J. Li, B. Xu, D. Li, M. P. Hautzinger, Y. Fu, T. Zhai, L. Xu, G. Niu, S. Jin and J. Tang, *Adv. Funct. Mater.*, 2018, **28**, 1704446.

33. T. P. Fehlner, M. Wu, B. J. Meneghelli and R. W. RUDOLPH, *Inorg. Chem.*, 1980, **19**, 49-54.

34. A. Yangui, S. Pillet, E.-E. Bendeif, A. Lusson, S. Triki, Y. Abid and K. Boukheddaden, *ACS Photonics*, 2018, **5**, 1599-1611.

35. A. Samet, A. B. Ahmed, A. Mlayah, H. Boughzala, E. K. Hlil and Y. Abid, *J. Mol. Struct.*, 2010, **977**, 72-77.

36. M. D. Smith and H. I. Karunadasa, *Acc. Chem. Res.*, 2018, **51**, 619-627.

37. E. R. Dohner, A. Jaffe, L. R. Bradshaw and H. I. Karunadasa, *J. Am. Chem. Soc.*, 2014, **136**, 13154-13157.

38. A. Vogler and H. Nikol, *Comment. Inorg. Chem.*, 1993, **14**, 245-261.

39. V. Morad, Y. Shynkarenko, S. Yakunin, A. Brumberg, R. D. Schaller and M. V. Kovalenko, *J. Am. Chem. Soc.*, 2019, **141**, 9764-9768.

40. Y. Jing, Y. Liu, J. Zhao and Z. Xia, *J. Phys. Chem. Lett.*, 2019, **10**, 7439-7444.

41. J. Lee, E. S. Koteles and M. O. Vassell, *Phys. Rev. B.*, 1986, **33**, 5512-5516.

42. N. Yamashita, O. Harada and K. Nakamura, *Jpn. J. Appl. Phys.*, 1995, **34**, 5539-5545.

43. V. Bachmann, C. Ronda and A. Meijerink, *Chem. Mater.*, 2009, **21**, 2077-2084.

44. J. M. Ogiegło, A. Zych, K. V. Ivanovskikh, T. Jüstel, C. R. Ronda and A. Meijerink, *J. Phys. Chem. A.*, 2012, **116**, 8464-8474.

45. K. M. McCall, C. C. Stoumpos, O. Y. Kontsevoi, G. C. B. Alexander, B. W. Wessels and M. G. Kanatzidis, *Chem. Mater.*, 2019, **31**, 2644-2650.

46. J. Luo, X. Wang, S. Li, J. Liu, Y. Guo, G. Niu, L. Yao, Y. Fu, L. Gao, Q. Dong, C. Zhao, M. Leng, F. Ma, W. Liang, L. Wang, S. Jin, J. Han, L. Zhang, J. Etheridge, J. Wang, Y. Yan, E. H. Sargent and J. Tang, *Nature*, 2018, **563**, 541-545.

47. D. Chen, S. Hao, G. Zhou, C. Deng, Q. Liu, S. Ma, C. Wolverton, J. Zhao and Z. Xia, *Inorg. Chem.*, 2019, **58**, 15602-15609.

48. R. Gautier, F. Massuyeau, G. Galnon and M. Paris, *Adv. Mater.*, 2019, **31**, e1807383.

49. L. Mao, P. Guo, M. Kepenekian, I. Hadar, C. Katan, J. Even, R. D. Schaller, C. C. Stoumpos and M. G. Kanatzidis, *J. Am. Chem. Soc.*, 2018, **140**, 13078-13088.

50. K. Robinson, G. V. Gibbs and P. H. Ribbe, *Science*, 1971, **172**, 567.

51. C. Zhou, M. Worku, J. Neu, H. Lin, Y. Tian, S. Lee, Y. Zhou, D. Han, S. Chen, A. Hao, P. I. Djurovich, T. Siegrist, M.-H. Du and B. Ma, *Chem. Mater.*, 2018, **30**, 2374-2378.

52. B. B. Cui, Y. Han, B. Huang, Y. Zhao, X. Wu, L. Liu, G. Cao, Q. Du, N. Liu, W. Zou, M. Sun, L. Wang, X. Liu, J. Wang, H. Zhou and Q. Chen, *Nat. Commun.*, 2019, **10**, 5190.

For Table of Contents Only

Two new hybrid metal halides $(PMA)_3BiBr_6$ and $(PMA)_3SbBr_6$ are obtained, and upon light excitation both exhibit broadband emission.